JOURNAL OF AIRCRAFT
Vol. 45, No. 2, March–April 2008

Flight-Loads Effects on Horizontal Tail Free-Play-Induced Limit Cycle Oscillation

P. C. Chen* and D. H. Lee†
ZONA Technology, Inc., Scottsdale, Arizona 85258

DOI: 10.2514/1.29611

The purpose of this paper is to study the impact of the flight-loads effects on the free-play-induced limit cycle oscillation using a direct simulation approach. This is achieved by computing the transient responses of an F-16 aeroelastic model with various free-play angles in its horizontal tails under various trim conditions, while subjected to external excitations due to gust or pilot input command. It is found that for the restrained structures, limit cycle oscillation always occurs, even with a very small free-play limit, as long as the horizontal tail is unloaded. However, once the horizontal tail is loaded at a trim condition, limit cycle oscillation disappears, even with a large free-play limit up to ±0.2 degrees. In contrast, for the unrestrained structures, even with large free-play limits up to ±0.1 degrees, limit cycle oscillation occurs only within a short period of time when the horizontal tail is unloaded. This is because for a free–free aircraft, when the horizontal tail is unloaded, the aircraft is untrimmed and then a transient maneuver will be developed and, consequently, the horizontal tail is rapidly loaded. In addition, it is unlikely that the F-16 can maintain an unloaded horizontal tail for a sufficiently long time until the limit cycle oscillation is fully developed. This suggests that the military specification for control surface free-play limit (±0.017 degrees) is probably too stringent for the F-16 and can be relaxed to reduce the manufacturing and maintenance costs.

Nomenclature

F_g	=	external loads including trim, maneuver, and gust loads
g	=	gravitational acceleration
$[K_{\text{free}}]$	=	stiffness matrix of the free–free horizontal tail structure
$[K_{\text{norm}}]$	=	stiffness matrices of the nominal structure
$\bar{K}_{\text{free}}$	=	generalized stiffness matrix of the free–free horizontal tail structure constructed using the fictitious mass modes
$\bar{K}_{\text{norm}}$	=	generalized stiffness matrix of the nominal structure constructed using the fictitious mass modes
M	=	Mach number
$[M_{\text{norm}}]$	=	mass matrices of the nominal structure
$\bar{M}_{\text{norm}}$	=	generalized mass matrix of the nominal structures constructed using the fictitious mass modes
$[\Delta M_{\text{FM}}]$	=	fictitious mass matrix.
N_z	=	translation acceleration along the z axis (load factor)
$\bar{Q}$	=	generalized aerodynamic force matrix constructed using the fictitious mass modes
q_∞	=	dynamic pressure
s_{free}	=	Laplace variable of the free–free horizontal tail flutter solution
s_{norm}	=	Laplace variable of the nominal structural flutter solution
θ	=	nonlinear parameter
θ_1, θ_2	=	free-play limit
$[\xi_{\text{FM}}]$	=	generalized coordinates of the fictitious mass modes
ξ_{free}	=	generalized coordinates of Φ_{free}
ξ_{norm}	=	generalized coordinates of Φ_{norm}
$[\Phi_{\text{FM}}]$	=	modal matrix of the sought fictitious mass modes
Φ_{free}	=	free–free horizontal tail structural modes obtained by the direct modal analysis
Φ_{norm}	=	nominal structural modes obtained by the direct modal analysis
ω_{FM}	=	natural frequencies of the fictitious mass model
ω_{free}	=	natural frequencies of the free–free horizontal tail structure
ω_{norm}	=	natural frequencies of the nominal structure

Presented as Paper 1851 at the 47th AIAA/ASME/ASCE/AHS/ASC Structures, Structural Dynamics, and Materials Conference, Newport, RI, 1–4 May 2006; received 5 January 2007; revision received 22 October 2007; accepted for publication 23 October 2007.

*Vice President, 9489 East Ironwood Square Drive, Suite 100. AIAA Member.

†Research and Development Engineering Specialist, 9489 East Ironwood Square Drive, Suite 100. AIAA Member.

I. Introduction

MANY studies have been performed on the limit cycle oscillation (LCO) phenomena of control surfaces that have structural nonlinearity, for example, free-play [1–7]. The wind-tunnel results obtained by Conner et al. [1], Hauenstein et al. [2], and McIntosh et al. [3] on a two-dimensional airfoil section, with free-play being incorporated either in the torsional spring or at the control surface hinge, show that LCO could occur at the speed below the linear flutter speed of the nominal structures. When the speed is increasing up to the linear flutter speed, the type of oscillatory response could evolve from a damped decay motion, periodic LCO, intermittent chaos, nearly harmonic LCO to divergent flutter. The numerical solutions obtained by Tang et al. [4,5] using a describing function method and by Price et al. [6,7] using a direct numerical integration approach demonstrated that these types of oscillatory responses due to free-play can be predicted by numerical methods.

LCO is a self-excited sustained vibration of limited amplitude which can impact on pilot handling quality, ride quality, and weapon aiming capability. It also can induce structural fatigue and, under some circumstances, flutter. Modern aircraft with control surfaces are often not balanced with balance weight to preclude flutter, but instead prevent flutter by relying on retained stiffness in powered actuators. Controlling free-play on these control surfaces becomes very important because they have a much larger destructive potential if free-play-induced LCO with sufficiently large amplitude occurs.

The military specification (MIL-SPEC) confines the free-play limit of all-moveable control surfaces to be within 0.034 deg (peak-to-peak value) to set the goal of no free-play-induced LCO during normal operation of aircraft. Usually, the manufacturing costs

increase as the free-play requirement becomes stricter. Therefore, it is highly desirable for this free-play limit to be relaxed while still ensuring the airplane to be free from LCO.

How much of the free-play limit can be relaxed probably depends on the aeroelastic characteristics of the aircraft. For instance, an F-16 was observed having a six-time free-play angle of the MIL-SPEC limit in its all movable horizontal tail (H.T.), but no LCO occurred during the flight. This gives rise to the following question: Is the current MIL-SPEC of free-play too strict or is the LCO suppressed by the flight loads on the H.T.? It is the purpose of this paper to answer these questions. This is achieved by performing the nonlinear flutter analysis for the F-16 with various H.T. free-play angles and under various maneuver conditions, subjected to various external excitations to study its LCO characteristics.

II. Nonlinear Flutter Methodology

Chen and Sulaeman [8] presented a direct simulation approach to solve the transient response of nonlinear aeroelastic systems. This direct simulation approach assumes that the nonlinearities in the aeroelastic system can be measured using a set of system parameters, called the nonlinear parameters. Any response of the system, such as displacement, velocity, or acceleration at structural grid points, structural element forces, component loads, sensor output, actuator input, etc., can be defined as nonlinear parameters. This leads to a set of piecewise discrete time-domain state-space equations. The transient response is solved by a direct time-integration procedure. At each time step, the value of the nonlinear parameter is first computed and then the time-integration procedure is switched to the corresponding state-space equation for the next time step. This nonlinear flutter methodology has been integrated into the ZAERO code [9]. The ZAERO code consists of many aeroelastic disciplines such as an unsteady aerodynamic module, a trim module, a transient maneuver loads module, a gust loads module, etc. The integrated nonlinear flutter and ZAERO code have become the ideal tool for the present free-play-induced LCO studies because various external excitations and trim conditions can be generated by ZAERO and applied to the nonlinear systems.

A. Structural and Aerodynamic Modeling of F-16 with Horizontal Tail Free-Play

Figure 1 presents an aerodynamic model of the F-16 aircraft which consists of 1716 aerodynamic boxes. The unsteady aerodynamic forces are generated using the ZONA6 method [10] in the ZAERO aerodynamic module. A structural finite element model of the F-16 provided by Lockheed Martin Aeronautics Company is shown in Fig. 2. Because the F-16 is a statically unstable aircraft, a time-domain simulation will definitely lead to a divergent response if the flight control system is not included in the simulation. To avoid the modeling of the flight control system for the simplification of the analysis, a 200 lb balance weight is added at the nose of the finite element model for generating a statically stable aircraft, so that only an open-loop analysis is sufficient for the present study.

The rotational degree of freedom (d.o.f.) of the structural grid point at the H.T. hinge line is selected as the nonlinear parameter. This divides the nonlinear structural system into two sublinear systems: one with the nominal structural stiffness matrix $[K_{\text{norm}}]$ and another with the free–free H.T. structural stiffness matrix $[K_{\text{free}}]$, and both are generated using MSC.NASTRAN [11]. Note that the free–free H.T. structural model is generated by setting a zero stiffness to the H.T. actuator. The modal approach is used to construct the state-space equations of the nominal and free–free H.T. structures. Thus, the size of the problem can be largely reduced from the number of degrees of freedom of the structural model to the number of structural modes. For the present study, it is found that the first 20 modes are sufficient for a converged solution. However, because the H.T. can experience an abrupt change of the deformation shape when the value of the nonlinear parameter crosses the free-play values, i.e., from a nearly rigid body pitch deformation to a nearly clamped torsion deformation, neither the mode shape of the free–free H.T. structure nor the nominal structure alone can be superimposed to accurately represent both deformed shapes of the H.T. within and without the free-play angle. Therefore, the modal approach raises an immediate technical issue regarding the selection of a set of structural modes that can best represent the physical d.o.f. in the entire nonlinear response domain. It is found that this technical issue can be circumvented using the fictitious mass method.

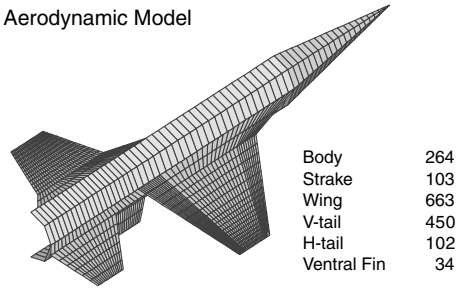

Fig. 1 Aerodynamic model of the F-16.

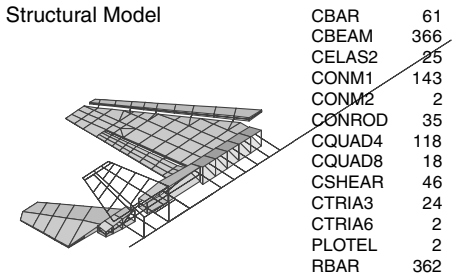

Fig. 2 Structural finite element model of the F-16.

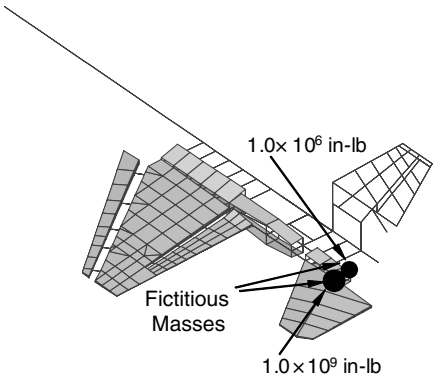

Fig. 3 Fictitious mass of the F-16 finite element model.

B. Fictitious Mass Method

The idea behind the fictitious mass (FM) method is a simple one [12]. First, a large mass is added at the d.o.f. in the finite element model where a large local deformation in the mode shape is desirable. These mode shapes are defined here as the FM modes. Then, this large mass is removed from the generalized mass matrix in the construction of the time-domain equations of motion so that the natural frequencies of the structures remain nearly unaltered. In so doing, these FM modes can represent the physical deformation more accurately than that of the natural modes of the structures if a large local deformation at the FM location is desired.

To apply the FM method, we added two large masses with inertia being equal to 10^9 in $\cdot$ lb$_f$ and 10^6 in $\cdot$ lb$_f$, respectively, at the rotation d.o.f. of the two grid points, as shown in Fig. 3. These two grid points are located at the endpoints of the bar elements that connect the H.T. and the fuselage. Because these two fictitious masses are sufficiently large, they can create a large distortion along this bar element and generate a nearly free–free pitch H.T. mode in one of the FM modes. These FM modes are computed by the following equation:

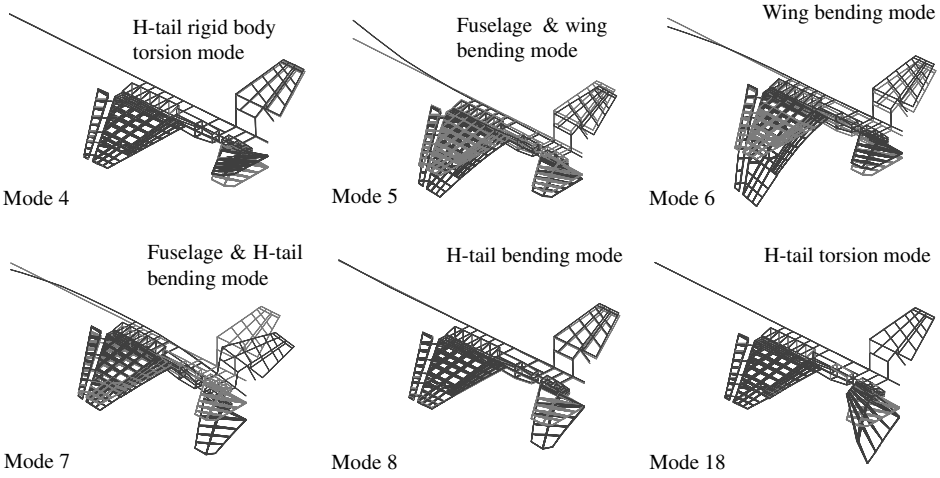

Fig. 4 Fictitious modes computed by the FM method.

$$[-\omega_{\mathrm{FM}}^2[M_{\mathrm{norm}} + \Delta M_{\mathrm{FM}}] + K_{\mathrm{norm}}][\Phi_{\mathrm{FM}}] = 0 \tag{1}$$

where $[M_{\mathrm{norm}}]$ and $[K_{\mathrm{norm}}]$ are the mass and stiffness matrices of the nominal structure, respectively, $[\Delta M_{\mathrm{FM}}]$ is the FM mass matrix, ω_{FM} is the natural frequencies of the fictitious mass model, and $[\Phi_{\mathrm{FM}}]$ is the modal matrix of the sought FM modes.

Figure 4 depicts the first six FM symmetric modes that contain the sought H.T. rigid body torsion mode and other elastic modes. Note that because of the free–free structural model, three symmetric rigid body modes are also obtained but they are not shown in Fig. 4. To verify that the FM modes do not alter the characteristics of the nominal structure and the free–free H.T. structure in a dynamic analysis, their natural frequencies are computed using Eqs. (2) and (3), respectively, which read

$$[-\omega_{\mathrm{norm}}^2\bar{M}_{\mathrm{norm}} + \bar{K}_{\mathrm{norm}}][\xi_{\mathrm{FM}}] = 0 \tag{2}$$

$$[-\omega_{\mathrm{free}}^2\bar{M}_{\mathrm{norm}} + \bar{K}_{\mathrm{free}}][\xi_{\mathrm{FM}}] = 0 \tag{3}$$

where $\bar{M}_{\mathrm{norm}} = [\Phi_{\mathrm{FM}}]^T[M_{\mathrm{norm}}][\Phi_{\mathrm{FM}}]$ and $\bar{K}_{\mathrm{norm}} = [\Phi_{\mathrm{FM}}]^T[K_{\mathrm{norm}}][\Phi_{\mathrm{FM}}]$ are the generalized mass and stiffness matrices, respectively, of the nominal structure constructed using the FM modes; $\bar{K}_{\mathrm{free}} = [\Phi_{\mathrm{FM}}]^T[K_{\mathrm{free}}][\Phi_{\mathrm{FM}}]$ is the generalized stiffness matrix of the free–free H.T. structure using the FM modes; $[\xi_{\mathrm{FM}}]$ is the generalized coordinates of the FM modes; ω_{norm} and ω_{free} are the natural frequencies of the nominal structure and the free–free H.T. structure, respectively.

These natural frequencies are then compared with those obtained by the direct modal analysis of the structures without the fictitious mass. This comparison is presented in Table 1, where very good agreement between the FM method and the direct modal analysis can be seen.

The final step to validate the FM method is the comparison between the flutter solutions computed using the FM modes and the modes obtained by the direct modal analysis. For the nominal structure, the flutter equations of these two sets of modes are presented in Eqs. (4) and (5), respectively.

$$[\Phi_{\mathrm{FM}}]^T(-s_{\mathrm{norm}}^2[M_{\mathrm{norm}}] + [K_{\mathrm{norm}}] - q_\infty[\mathrm{AIC}])[\Phi_{\mathrm{FM}}]\{\xi_{\mathrm{FM}}\} = 0 \tag{4}$$

$$[\Phi_{\mathrm{norm}}]^T(-s_{\mathrm{norm}}^2[M_{\mathrm{norm}}] + [K_{\mathrm{norm}}] - q_\infty[\mathrm{AIC}])[\Phi_{\mathrm{norm}}]\{\xi_{\mathrm{norm}}\} = 0 \tag{5}$$

where s_{norm} is the Laplace variable of the nominal structural flutter solution, q_∞ is the dynamic pressure, Φ_{norm} is the nominal structural modes obtained by the direct modal analysis, ξ_{norm} is the generalized coordinates of Φ_{norm}, and AIC is the aerodynamic influence coefficient matrix computed by the ZONA6 method.

For the free–free H.T. structure, the flutter equations read

$$[\Phi_{\mathrm{FM}}]^T(-s_{\mathrm{free}}^2[M_{\mathrm{norm}}] + [K_{\mathrm{free}}] - q_\infty[\mathrm{AIC}])[\Phi_{\mathrm{FM}}]\{\xi_{\mathrm{FM}}\} = 0 \tag{6}$$

$$[\Phi_{\mathrm{free}}]^T(-s_{\mathrm{free}}^2[M_{\mathrm{norm}}] + [K_{\mathrm{free}}] - q_\infty[\mathrm{AIC}])[\Phi_{\mathrm{free}}]\{\xi_{\mathrm{free}}\} = 0 \tag{7}$$

where s_{free} is the Laplace variable of the free–free H.T. flutter solution, Φ_{free} is the free–free H.T. structural modes obtained by the direct modal analysis, and ξ_{free} is the generalized coordinates of Φ_{free}.

Equations (4–7) are then solved using the g-method [13] whose solutions at $M = 0.8$ are presented in Fig. 5. By comparing the results to the direct modal analysis, it can be seen that the FM method captures the aeroelastic characteristics of the nominal and free–free H.T. structures accurately. Note that the direct modal analysis shown in Eqs. (5) and (7) for the flutter analysis of the nominal structure and the free–free H.T. structure requires different generalized coordinates ξ_{norm} and ξ_{free}. If this direct modal analysis is adopted for a nonlinear flutter analysis, it can create a discontinuous structural deformation when the H.T. rotation crosses the free-play angle which is not physical. In contrast, the FM method employs only one set of generalized coordinates ξ_{FM} for both the nominal structure and the free–free H.T. structure, which ensures a continuous structural deformation in the time-integration procedure.

Table 1 Comparison of natural frequencies by FM and direct methods

	Nominal structures		Free–free H.T. structures	
Mode no.	Direct	Fictitious mass mode	Direct	Fictitious mass mode
1	0.00	——	0.00	——
2	0.00	0.00	0.00	0.00
3	0.00	0.02	0.00	0.02
4	8.68	8.68	0.04	0.27
5	10.60	10.60	8.70	8.70
6	18.44	18.44	10.77	10.77
7	23.22	23.22	21.30	21.30
8	26.86	26.86	26.38	26.38
9	32.33	32.33	29.29	29.30
10	44.47	44.47	32.37	32.37

C. Formulation of the Free-Play-Induced Limit Cycle Oscillation Analysis

By defining the difference in the rotation d.o.f. between the two grid points where the fictitious masses are located as the nonlinear parameter θ, the nonlinear systems can be divided into three sublinear systems as shown in Fig. 6, and their corresponding equations of motion are presented in Eq. (8).

$$[\bar{M}_{\mathrm{norm}}]\{\ddot{\xi}_{\mathrm{FM}}\} + [\bar{K}_{\mathrm{norm}}]\{\xi_{\mathrm{FM}}\} - q_\infty[\bar{Q}]\{\xi_{\mathrm{FM}}\} = F_g + [\Phi_{\mathrm{FM}}]^T[K_{\mathrm{norm}}]\{\theta_2\} \qquad \theta > \theta_2 \tag{8a}$$

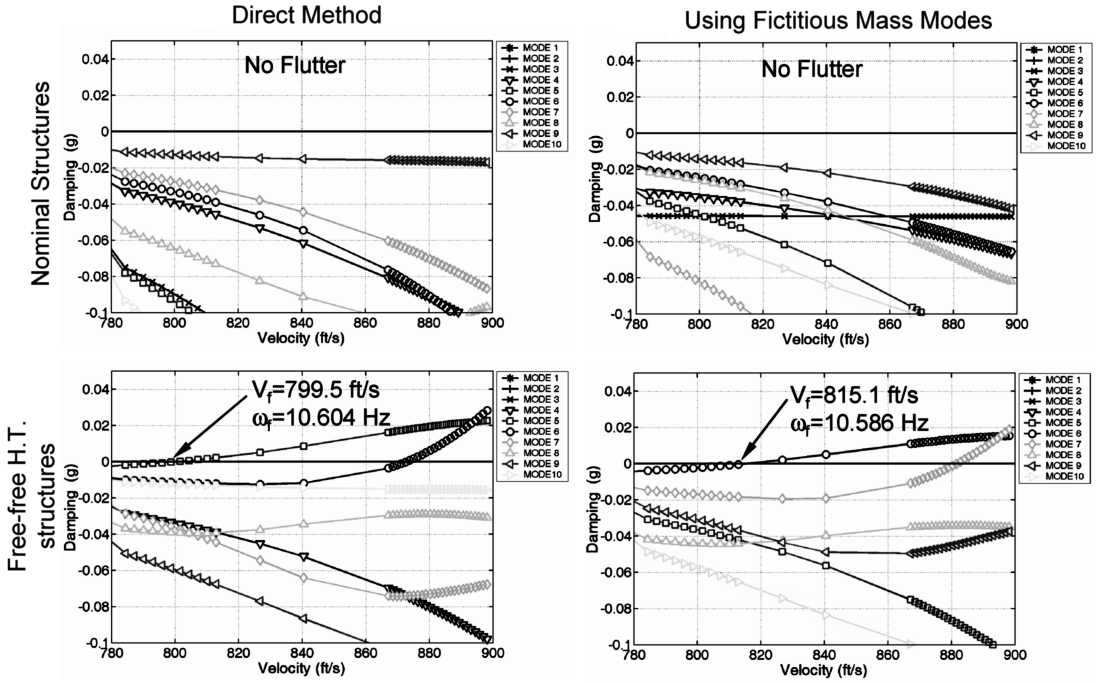

Fig. 5 Flutter solutions at $M = 0.8$ of the nominal and free–free H.T. structures.

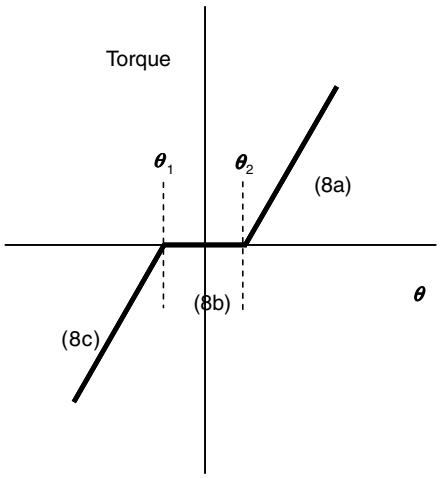

Fig. 6 Three sublinear systems for the F-16 structures with H.T. free-play.

$$[\bar{M}_{\text{norm}}]\{\ddot{\bar{\xi}}_{\text{FM}}\} + [\bar{K}_{\text{free}}]\{\xi_{\text{FM}}\} - q_\infty[\bar{Q}]\{\xi_{\text{FM}}\} = F_g \qquad \theta_1 \le \theta \le \theta_2 \tag{8b}$$

$$[\bar{M}_{\text{norm}}]\{\ddot{\bar{\xi}}_{\text{FM}}\} + [\bar{K}_{\text{norm}}]\{\xi_{\text{FM}}\} - q_\infty[\bar{Q}]\{\xi_{\text{FM}}\} = F_g - [\Phi_{\text{FM}}]^T[K_{\text{norm}}]\{\theta_1\} \qquad \theta < \theta_1 \tag{8c}$$

where $\theta_1 \le \theta \le \theta_2$ is the free-play limit; $\bar{Q} = [\Phi_{\text{FM}}]^T[AIC][\Phi_{\text{FM}}]$ is the generalized aerodynamic force matrix; F_g is the external loads including trim loads, maneuver loads, and gust loads; and $[\Phi_{\text{FM}}]^T[K_{\text{norm}}]\{\theta_1\}$ and $[\Phi_{\text{FM}}]^T[K_{\text{norm}}]\{\theta_2\}$ are the offset moments.

The generalized aerodynamic force matrix is recast into a rational function using the minimum state method [14], getting a set of time-domain state-space equations ready for a time-integration computation. At each time step, the value of the nonlinear parameter is first calculated, then the time-integration scheme is switched to its corresponding sublinear system for the time marching of the next time step. In addition, at each time step, the external excitation either from the gust or pilot input command is generated using the ZAERO gust or maneuver loads modules, respectively. Initial trim condition, for instance, a given load factor N_z, also can be specified and solved by the ZAERO trim module. This trim solution in terms of trimmed angle of attack, H.T. deflection angle, and the modal displacement are used as the initial condition of the transient response analysis. It should be noted that, under a trim condition, an infinitesimal trim load on the H.T. is sufficient to push the H.T. to the boundary of the free-play limit. The remaining trim loads are balanced by the elastic forces from the nominal structures. Therefore, the nominal structure is used to solve the trim condition. This also shifts the free-play limit from $-\theta_0 < \theta < \theta_0$ to $0 < \theta < 2\theta_0$, where θ_0 represents the free-play limit without the trim loads.

III. Numerical Results

A. Scenarios for the Free-Play-Induced Limit Cycle Oscillation Analysis

Two types of F-16 structures are modeled for the free-play-induced LCO analysis. One is the restrained structures (without the rigid body modes) and the other is the unrestrained structures (with rigid body modes). The restrained structures can simulate a sting-supported wind-tunnel model, whereas the unrestrained structures are used to simulate free–free aircraft. The transient responses of the both restrained and unrestrained structures are computed at various flight conditions while subjected to a gust excitation or a pilot command. These conditions are summarized in Table 2.

The transient responses include the root mean square (rms) of the H.T. leading edge (L.E.) displacement, the H.T. rotation angle, and the H.T. hinge moment. These transient responses are used to identify the flight-loads effects on LCO. All flight conditions are assumed to be at Mach number 0.8 and 10,000 ft altitude.

B. Restrained Structures at $N_z = 0$ g Subjected to Gust Excitation (Case 1)

This analysis condition is very similar to the wind-tunnel test of a wing with structural nonlinearity at rotational hinge, and the wing is mounted vertically in the wind tunnel to simulate unloaded condition of the wing.

Figure 7 presents the transient response of the H.T. rotation angle at $N_z = 0$ g subjected to one-minus-cosine gust with gust velocity $=$ 20 ft/s and at ± 0.017, ± 0.10, and ± 1.0 deg of free-play. Because the H.T. is nearly unloaded at $N_z = 0$ g, it can be seen that LCO is unavoidable even with the MIL-SPEC free-play limits

Table 2 Scenarios with various flight conditions and excitations

Aircraft state	Flight condition	Excitation	Case
Restrained	AoA = 0.0 deg, H.T. = 0.0 deg	gust	case 1
	AoA = 1.4 deg, H.T. = 0.0 deg	pilot input	case 2
	Various AoA, H.T. = 0.0 deg	gust	case 3
Unrestrained	N_z = 1.0 g, AoA = 1.26 deg, H.T. = 0.96 deg	gust	case 4
	N_z = 1.0 g, AoA = 1.855 deg, H.T. = −1.386 deg	pilot input	case 5

(±0.017 deg). It is also found that the maximum rotation angle is approximately twice the free-play limit. This suggests that, as long as free-play exists and the structure is subjected to an unloaded condition, LCO could occur regardless how small the free-play is.

C. Restrained Structures at Trimmed Angle of Attack Subjected to Pilot Input Command (Case 2)

This analysis case is to investigate how the loaded and unloaded conditions of the H.T. affect the LCO. In this case, a ZAERO trimmed analysis is first performed. The computed trim angle of attack ($\alpha = 1.4$ deg) and the trimmed structural deformation are used as the initial trim condition for the LCO analysis. The pilot input command, in terms of the H.T. rotation-angle time history shown in Fig. 8a, is used to excite the structures. For a ±0.2 deg of free-play limit, the transient response of the H.T. rotation angle is present in Fig. 8b. It can be seen that LCO occurs during the duration of the positive command, e.g., at 0.4–1.4 s and at 2.3–3.2 s, but it stops at the negative pilot input command, e.g., at 1.5–2.2 s and 3.3–3.9 s. Also, LCO disappears after the pilot input command vanishes. To understand this phenomena, we have calculated the hinge moment of the H.T. at $\alpha = 1.4$ deg with a zero deflection angle and with a 1 deg pitch-up angle. This calculation shows that the H.T. has a negative hinge moment at zero deflection angle and a positive hinge moment at a 1 deg pitch-up angle. This implies that the H.T. must experience an unloaded condition when its deflection increases from 0 deg to a 1 deg pitch-up angle. This unloaded condition triggers the occurrence of LCO. Once LCO occurs, it continues as long as the H.T. is in the positive pitch-up condition, because the H.T. is only slightly loaded in this condition. This LCO can be suppressed only when the H.T. is at the zero or pitch-down deflection angle because the pitch-down deflection angle adds more negative hinge moment to that of the zero deflection angle. Therefore, this large negative hinge moment stops the LCO while the H.T. is in the pitch-down condition.

D. Restrained Structures at Various Angles of Attack and Free-Play Limits (Case 3)

Figure 9 presents the rms values of the L.E. tip displacement of the H.T. at various angles of attack and free-play limits, while subjected to a 50 ft/s one-minus-cosine gust. It can be seen that the rms value increases as the free-play increases. On the other hand, the rms value decreases as the angle of attack increases. It is interesting to see that at the MIL-SPEC limit (±0.017 deg), LCO vanishes as long as the H.T. is slight loaded ($\alpha = 0.2$ deg). In addition, LCO also vanishes if the angle of attack exceeds 1.4 deg even with a free-play limit up to ±0.2 deg.

To study the sensitivity of LCO to the change of angle of attack and free-play angle, three cases corresponding to points A, B, and C shown in Fig. 9 at the LCO boundary are selected whose free-play angles and angles of attack are presented in Table 3. The transient responses in terms of H.T. hinge moment (torque) and rotation angle of the three cases when subjected to a 50 ft/s one-minus-cosine gust are depicted in Fig. 10.

In this study, both upward and downward gusts are analyzed, where the downward gust is found to be the more critical case. At ±0.1 deg of free-play and 0.8 deg of angle of attack, LCO occurs (Fig. 10b). But with a slight decrease of free-play angle (Fig. 10a) or a slight increase of angle of attack (Fig. 10c), LCO disappears. These

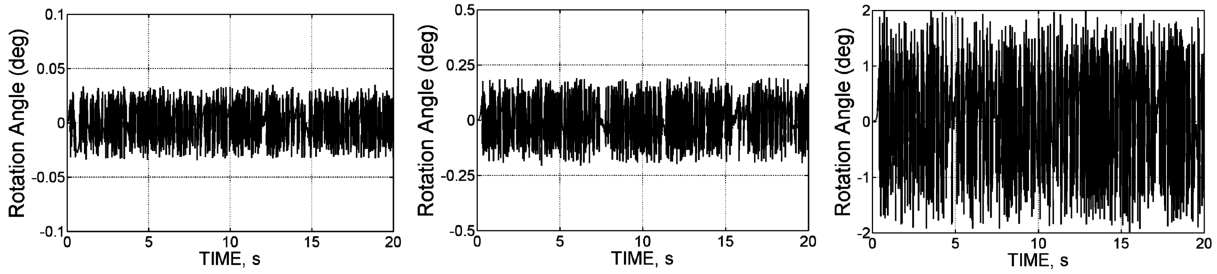

Fig. 7 Transient response of the restrained structures subject to gust excitation at various free-play angles.

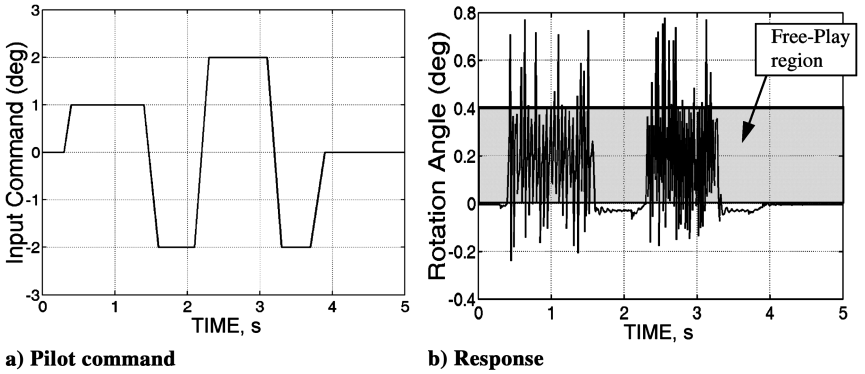

Fig. 8 Transient response of restraint structures subjected to pilot input command with free-play limit = ±0.2 deg.

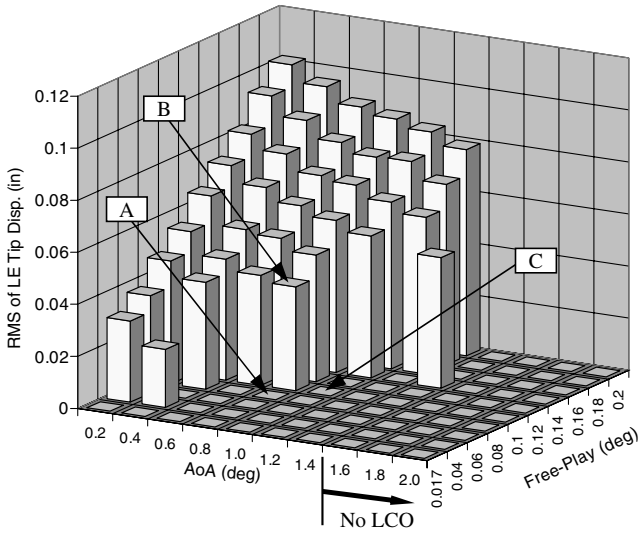

Fig. 9 RMS of the H.T. displacement at various angles of attack and free-play limits.

Table 3 Three down selected conditions to investigate LCO due to AoA and free-play angle

Case	Free-play angle, deg	Angle of attack, deg
Point A	±0.08	0.8
Point B	±0.1	0.8
Point C	±0.1	1.0

results clearly demonstrate the sensitivity of LCO to the change of free-play limit and angle of attack.

E. Unrestrained Structures at 1 g Trim Condition Subjected to Gust (Case 4)

Two rigid body modes, namely the plunge and pitch modes, are included in the unrestrained structures. The generalized coordinates of those two rigid body modes are transformed into four airframe states, namely angle of attack, altitude, pitch rate, and flight path angle, using the technique described in [15]. The ZAERO trim solution shows that, at $M = 0.8$ and sea level, the trim angle of attack is 1.26 deg and the H.T. deflection angle is -0.96 deg. This trim condition also produces a -976 in $\cdot$ lb of H.T. hinge moment. The transient response at ± 0.017, ± 0.1, and ± 1.0 deg of free-play limits while subjected to a 50 ft/s gust are shown in Fig. 11. It can be seen

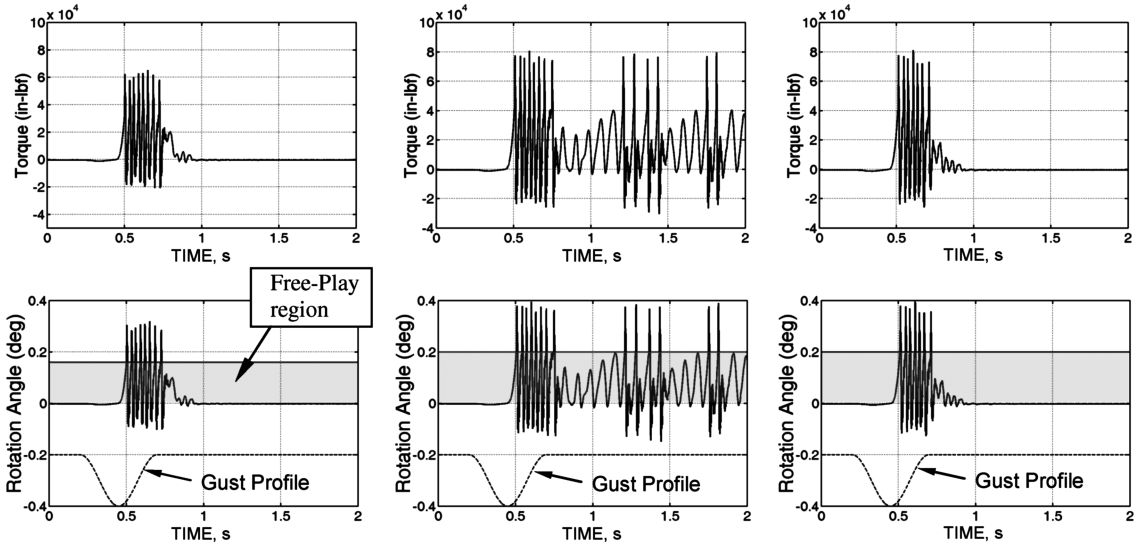

a) ±0.08 free-play AoA=0.8 deg. (Point A)

b) ±0.10 free-play AoA=0.8 deg. (Point B)

c) ±0.10 free-play AoA=1.0 deg. (Point C)

Fig. 10 Sensitivity of LCO to the free-play limit and angle of attack.

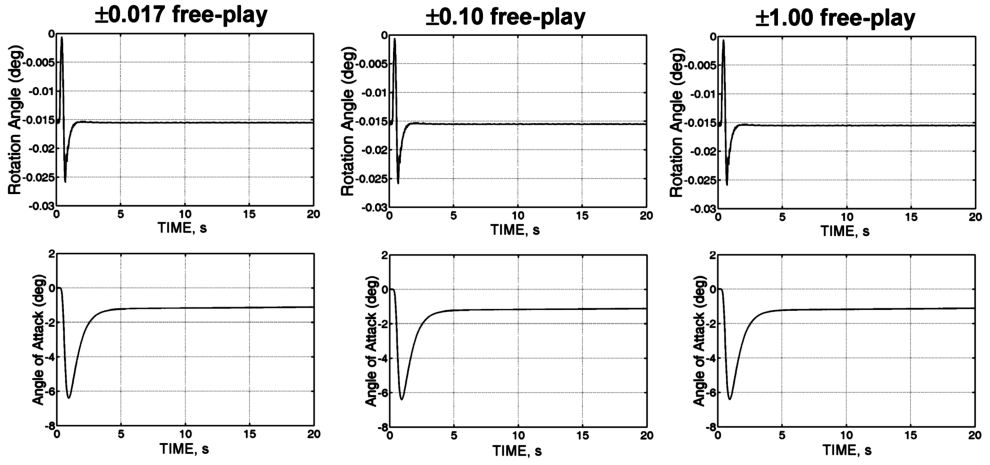

Fig. 11 Unrestrained structures 1 g trim condition and various free-play limits subjected to 50 ft/s gust.

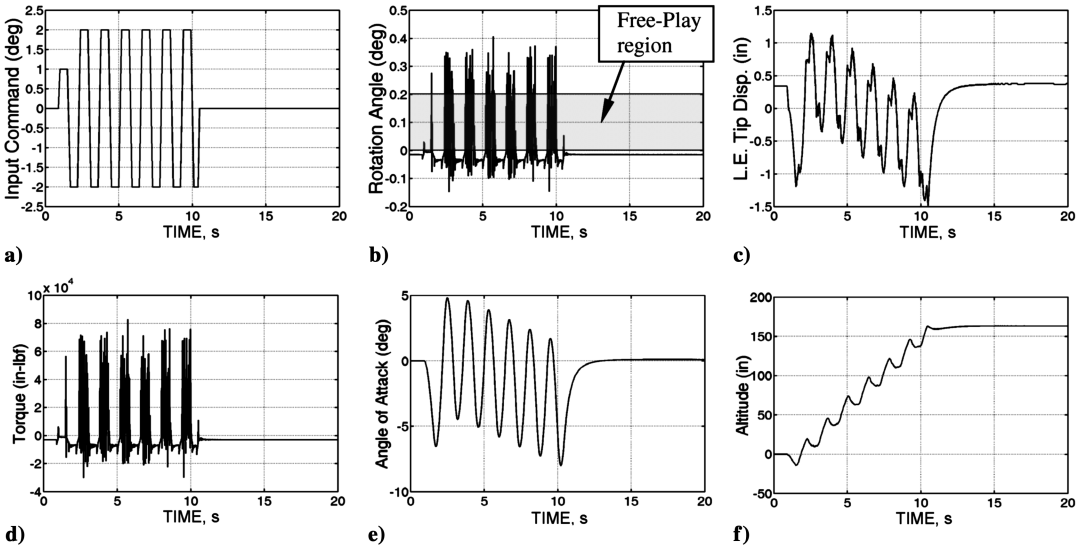

Fig. 12 Unrestrained structures subjected to pilot input command at ±0.1 deg of free-play limit.

that no LCO occurs even with the free-play limit up to ± 1.0 deg. Note that the rotation-angle time history shown in Fig. 11 is the rotation of the H.T. at hinge due to the elastic deformation, which excludes the deflection angle due to trim. This transient result shows that the 50 ft/s gust excitation is not strong enough to overcome the -976 in · lb of hinge moment due to the trim loads. In other words, the rotation angle remains negative and does not cross through the zero deflection position. Thereby, the H.T. is always loaded, which suppresses the LCO.

F. Unrestrained Structures Subjected to Pilot Input Command (Case 5)

Figure 12a presents the time history of the H.T. deflection angle commanded by pilot input. This pilot input can produce a series of pitch-up and pitch-down motions of the aircraft that periodically unloads the H.T. The transient responses of the H.T. rotation angle, L.E. tip displacement, torque, angle of attack, and altitude, at ± 1.0 deg of free-play limit are shown in Figs. 12b–12f, respectively. It can be seen that LCO occurs only during the short period when the H.T. is unloaded, but it disappears after the pilot input command finishes, suggesting that LCO cannot be sustained even if the pilot intentionally unloads the H.T. This is because when the H.T. is unloaded, the aircraft is untrimmed which consequently induces a transient motion of the aircraft. During this transient motion, the H.T. will be rapidly loaded again.

This study shows that, as long as a loaded H.T. is required for trim, free-play cannot induce a sustained LCO. However, if there exists a flight condition where a trim condition can be achieved without a loaded H.T., one can modify the flight condition law for this flight condition, such that a small deflection is introduced to another control surface, for instance the wing trailing-edge flap. In so doing, the aerodynamic center of the whole aircraft shifts to avoid the unloaded H.T. condition for trim.

IV. Conclusions

The present study shows that, for the restrained F-16 structures at $N_z = 0$ g, the H.T. free-play could induce LCO even with very small free-play. But, LCO disappears when the H.T. is loaded. However, for the unrestrained F-16 structures even with large free-play, LCO occurs only within a short period of time when the H.T. is unloaded. This is because, for a free–free aircraft when the H.T. is unloaded, the aircraft is untrimmed and transient motion will be developed and, consequently, rapidly load the H.T. In addition, it is unlikely that the F-16 can maintain an unloaded H.T. for a sufficiently long time until the LCO is fully developed. This probably can explain why an F-16 was observed having a six-time free-play angle of the MIL-SPEC limit, but no LCO occurred during the flight.

The present study also suggests that the current MIL-SPEC can probably ensure the elimination of LCO for a restrained aircraft as long as the H.T. is loaded. But the current MIL-SPEC is too stringent for a free–free aircraft (unrestrained structures) if a loaded H.T. is always required for trim in all flight conditions. Therefore, before the MIL-SPEC can be relaxed for a particular aircraft, one must conduct a massive number of flight dynamics simulations to search for a flight condition where the H.T. is only slightly loaded. If such a flight condition exists, one could modify the flight control law such that another control surface is deflected to shift the aerodynamic center. In this case, a loaded H.T. would be required to counterbalance such a shift of aerodynamic center, ensuring a loaded H.T. in all flight conditions. However, how much the free-play limit can be relaxed from the current MIL-SPEC limit must be carefully analyzed by means of numerical simulation or wind-tunnel testing.

References

[1] Conner, M. D., Tang, D. M., Dowell, E. H., and Virgin, L. N., "Nonlinear Behavior of a Typical Airfoil Section with Control Surface Freeplay: A Numerical and Experimental Study," *Journal of Fluids and Structures*, Vol. 11, No. 1, Jan. 1997, pp. 89–109. doi:10.1006/jfls.1996.0068

[2] Hauenstein, A. J., Zara, J. A., Eversman, W., and Qumei, I., "Chaotic and Nonlinear Dynamic Response of Aerosurfaces with Structural Nonlinearities," AIAA Paper 92-2547, April 1992.

[3] McIntosh, S. C., Jr., Reed, R. E., Jr., and Rodden, W. P., "Experimental and Theoretical Study of Nonlinear Flutter," *Journal of Aircraft*, Vol. 18, No. 12, Dec. 1981, pp. 1057–1063.

[4] Tang, D., Kholodar, D., Dowell, E. H., "Nonlinear Response of Airfoil Section with Control Surface Freeplay to Gust Loads," *AIAA Journal*, Vol. 38, No. 9, 2000, pp. 1543–1557.

[5] Tang. D., Dowell, E. H., and Virgin, L. N., "Limit Cycle Behavior of an Airfoil with a Control Surface," *Journal of Fluids and Structures*, Vol. 12, No. 7, Oct. 1998, pp. 839–858. doi:10.1006/jfls.1998.0174

[6] Price, S. J., Alighanbari, H., and Lee, B. H. K., "Aeroelastic Response of a Two-Dimensional Airfoil with Bilinear and Cubic Structural Nonlinearities," *Journal of Fluids and Structures*, Vol. 9, No. 2, Feb. 1995, pp. 175–193. doi:10.1006/jfls.1995.1009

[7] Price, S. J., Lee, B. H. K., and Alighanbari, H., "Postinstability Behavior of a Two-Dimensional Airfoil with a Structural Nonlinearity," *Journal of Aircraft*, Vol. 31, No. 6, 1994, pp. 1395–1401.

[8] Chen, P. C., and Sulaeman, E., "Nonlinear Response of Aeroservoelastic Systems Using Discrete State-Space Approach," *AIAA Journal*, Vol. 41, No. 9, Sept. 2003, pp. 1658–1666.

[9] Anon., ZAERO Software Package, Ver. 8.1, ZONA Technology, Scottsdale, AZ, July 2007.

[10] Chen, P. C., Lee, H. W., and Liu, D. D., "Unsteady Subsonic Aerodynamics for Bodies and Wings with External Stores Including Wake Effect," *Journal of Aircraft*, Vol. 30, No. 5, 1993, pp. 618–628.
[11] Anon., MSC.NASTRAN Software Package, Ver. 2004, MSC.Software, Santa Ana, CA, 2004.
[12] Karpel, M., and Presente, E., "Structural Dynamic Loads in Response to Impulsive Excitation," *Journal of Aircraft*, Vol. 32, No. 4, 1995, pp. 853–861.
[13] Chen, P. C., "Damping Perturbation Method for Flutter Solution: the g-Method," *AIAA Journal*, Vol. 38, No. 9, 2000, pp. 1519–1524.
[14] Karpel, M., "Extensions to the Minimum-State Aeroelastic Modeling Method," *AIAA Journal*, Vol. 29, No. 11, 1991, pp. 2007–2009.
[15] Baldelli, D. H., Chen, P. C., and Panza, J., "From Aeroelastic Formulation To Flight Dynamic Equations and Its Application to Predator UAV," *CEAS/AIAA/DGLR International Forum on Aeroelasticity and Structural Dynamics*, IF-104, 2005.